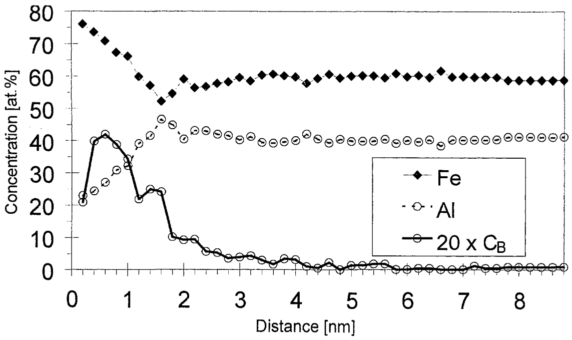

Fig. 4. Radial distributions of Fe, Al, and B (concentration in atomic percent, multiplied by 20 for boron) with respect to the center of the boron atmosphere. Boron segregation extends up to 3 nm from the dislocation core. Calculated concentrations (C) are subject to sampling errors, which gradually decrease with r according to the relation $\delta C \sim [C(1 - C)/N]^{1/2}$, where the number of ions (N) is proportional to r^2. The statistical fluctuations related to the maximum boron concentration (2 atomic %) are close to 1 atomic %.

local curvature of planes in the close vicinity of the end of the extra half-plane, in good agreement with geometrical descriptions of edge dislocations.

The B-enriched pipe-shaped zone, parallel to the dislocation line, is detected in the vicinity of the extremity of the additional half-plane (Fig. 3). This image therefore provides evidence that the B-enriched zone shown in Fig. 2 is a Cottrell atmosphere. Interstitial atoms like boron are likely to segregate under the dislocation line, in the dilated region of the defect. Therefore, a plausible location of the dislocation could be around 1 nm above the center of the atmosphere (Fig. 3). However, the exact location of the dislocation line in the reconstructed image is difficult to ascertain with certainty.

The position of the B-rich pipe, slightly to the right of the apparent position of the dislocation line, is a priori surprising. However, reconstructed images must be interpreted with caution. The applied stress caused by the high electric field may have led to a partial breakaway of the dislocation from its atmosphere during the investigation, resulting in a shift of the line defect by a few atomic planes toward the specimen surface (left side, Figs. 2 and 3). Preferential retention of boron from one plane to the next may also shift boron slightly (0.15 nm) to the left in Fig. 3.

Radial distributions of atomic species (Fig. 4) with respect to the center of mass of the atmosphere (that is, the axis of the boron "finger" shown in Fig. 2) were calculated in successive shells of equal thickness (0.2 nm). The maximum concentration of boron C_B is close to 2 atomic %. The extent of the atmosphere, taken at one-tenth of the maximum boron concentration (that is, $C_B = 0.2$ atomic %), can be estimated at 3 nm.

In a first approximation, the interstitial concentration C_B at a given temperature T in the strain field of a dislocation can be written as $C_B = C^0 \exp(u/kT)$, where C^0 is the nominal boron concentration (400 atomic ppm), u is the binding energy between the dislocation and interstitial, and k is the Boltzmann constant. From the present measurements we estimate $u \approx 0.2$ eV, a reasonable value compared to the binding energy of carbon in iron (~0.5 eV). [A more detailed interpretation using recent models (*11, 12*) has not yet been offered.] One feature in Fig. 4 is unexpected: The Al concentration falls at the center of the atmosphere (20 atomic %, as compared to 40 atomic % in the bulk).

Similar atmospheres were encountered during the systematic experiments that were carried out. Among the three boron-enriched clouds that could be found, only one could be interpreted quantitatively on a sound basis. This atmosphere appeared as a rod-shaped zone containing 6 atomic % boron. Similar to what is shown in Fig. 4, the boron-enriched zone was Al-depleted (33 atomic %). Its diameter was close to 3 nm. Unfortunately, the dislocation line associated with this atmosphere could not be imaged.

The information revealed by 3DAP on the spatial distribution of chemical species near line defects is important both from an academic point of view and for applications. The observed modifications of concentrations close to dislocation lines evidently alter the core structure of defects, which in turn has a great influence on the plasticity behavior of material. The existence of the unexpected Al depletion within Cottrell atmospheres is an intriguing phenomenon that remains to be explained.

References

1. A. H. Cottrell and B. A. Bilby, *Proc. Phys. Soc. London Ser. A* **62**, 49 (1949).
2. M. K. Miller, A. Cerezo, M. G. Hetherington, G. D. W. Smith, *Atom Probe Field Ion Microscopy* (Clarendon, Oxford, 1996).
3. L. Chang, S. J. Barnard, G. D. W. Smith, in *Fundamentals of Aging and Tempering in Bainitic and Martensitic Steel Products*, G. Klaus and P. E. Repas, Eds. (Iron & Steel Society, Warrendale, PA, 1992), pp. 19–28.
4. R. Jayaram and M. K. Miller, *Scr. Metall. Mater.* **33**, 19 (1995).
5. D. Blavette, A. Bostel, J. M. Sarrau, B. Deconihout, A. Menand, *Nature* **363**, 432 (1993).
6. A. Cerezo, T. J. Godfrey, G. D. W. Smith, *Rev. Sci. Instrum.* **59**, 862 (1988).
7. M. A. Crimp and K. Vedula, *Mat. Sci. Eng.* **78**, 193 (1986).
8. A. Fraczkiewicz, A.-S. Gay, M. Biscondi, *J. Phys. IV* **9**, 75 (1999).
9. D. Blavette, B. Deconihout, S. Chambreland, A. Bostel, *Ultramicroscopy* **70**, 115 (1998).
10. M. A. Morris and D. G. Morris, *Scr. Metall. Mater.* **38**, 509 (1998).
11. A. S. Nandedkar and R. A. Johnson, *Acta Met.* **30**, 2055 (1982).
12. W. G. Wolfer and M. I. Baskes, *Acta Met.* **33**, 2005 (1985).

6 September 1999; accepted 10 November 1999

Deflection of the Local Interstellar Dust Flow by Solar Radiation Pressure

M. Landgraf,[1,2]* K. Augustsson,[3] E. Grün,[4] B. Å. S. Gustafson[5]

Interstellar dust grains intercepted by the dust detectors on the Ulysses and Galileo spacecrafts at heliocentric distances from 2 to 4 astronomical units show a deficit of grains with masses from 1×10^{-17} to 3×10^{-16} kilograms relative to grains intercepted outside 4 astronomical units. To divert grains out of the 2– to 4–astronomical unit region, the solar radiation pressure must be 1.4 to 1.8 times the force of solar gravity. These figures are consistent with the optical properties of spherical or elongated grains that consist of astronomical silicates or organic refractory material. Pure graphite grains with diameters of 0.2 to 0.4 micrometer experience a solar radiation pressure force as much as twice the force of solar gravity.

Identical dust impact detectors (*1, 2*) were installed on the Ulysses spacecraft, which flies in a polar orbit around the sun, and on the Galileo spacecraft, which continues to fly in a jovian orbit. The instruments sense the plasma cloud generated as individual dust grains strike a detector plate at high velocity. Independent impact plasma charge measurements distinguish real events from spurious recordings and were used to derive the grain mass and impact velocity (*3*).

The Ulysses and Galileo dust measurements were mainly designed to reveal the spatial distribution of interplanetary dust grains that are released from minor solar system objects like asteroids and comets (*4*).

But in the data transmitted back from the spacecrafts, two new classes of cosmic dust in the solar system were discovered: periodic streams of small grains [diameter 5 to 10 nm (*5*)] originating from the jovian system, and a flow of interstellar grains traversing the solar system on unbound orbits (*6*). The in situ data allow interstellar and interplanetary grains to be distinguished by their nearly opposite impact direction (*7*). The flow of interstellar grains was found to come from the same direction [~259° heliocentric ecliptic longitude and 8° latitude (*8*)] as the stream of neutral interstellar gas, consisting mainly of hydrogen and helium, that passes by the sun on its way through the local interstellar cloud (LIC) (*9–12*). The interstellar origin of the newly discovered grain population was confirmed by an average orbital velocity that exceeded the local solar system escape velocity (*7*) and a nearly constant impact rate at all ecliptic latitudes (*13*).

Model calculations accounting for solar gravitation and the radiation pressure force due to sunlight (*14*) indicated that interstellar grains smaller than ~0.04 μm in diameter may be concentrated in the sun's wake in the same way as the gas. However, a concentration of small interstellar grains could not be detected by the dust instruments on the Pioneer 8 and 9 spacecrafts (*15*). The nondetection of such small interstellar grains in the solar system was explained by Levy and Jokipii (*16*), who pointed out that the grains acquire a net charge by photoelectron emission and are dispersed by the solar wind magnetic field. However, the effects of the solar wind magnetic field are limited at low heliographic latitudes as sectors of opposite polarity sweep by the dust grains. Because these reversals of the field happen on time scales of the solar rotation period [average about 27 days (*17*)], which is short relative to a grain's gyro-period [about 35 years (*7*)], the grains' motion depends on the average rather than the instantaneous force (*18*). At low heliographic latitudes, sectors of positive and negative polarity nearly cancel each other such that the average field is much weaker than the instantaneous one. This is relevant because the interstellar stream direction is within 10° of the solar equatorial plane (*19*). The net effect of the solar wind magnetic field is either to concentrate grains to the equatorial plane or to divert them from the plane, depending on the phase of the 22-year solar magnetic cycle (*18, 20, 21*).

We have isolated the interstellar grain population in the Ulysses and Galileo in situ data and analyzed its properties. The measured mass distribution of interstellar grains, as detected by Ulysses and Galileo, ranges from 10^{-18} to 10^{-12} kg and peaks near 10^{-16} kg (Fig. 1). For masses larger than 3×10^{-16} kg, the corresponding cumulative distributions can be described analytically using a power-law function with a negative exponent of −0.90 (*22*). The lower cutoff of the measured mass distribution is determined by the detection threshold of the Ulysses and Galileo dust detectors, which is 10^{-18} kg at the ~20 km s^{-1} impact speeds of the interstellar grains.

The shape of the mass distribution of grains detected by Ulysses outside 4 astronomical units (AU) (Fig. 1B) is similar to the shape of the mass distribution of all grains detected in situ by Ulysses and Galileo (Fig. 1, A and E). However, grains detected by Ulysses between 2 and 4 AU (Fig. 1C) are less abundant in the mass range from 1×10^{-17} to 3×10^{-16} kg (diameter range 0.2 to 0.6 μm for spherical particles with a mass density of 2500 kg m^{-3}). To compare the histograms in Fig. 1, B and C, we corrected (*23*) for the differences in exposure times and subtracted them from each other (Fig. 1D). For large grains (mass > 3×10^{-15} kg), we see no difference between the distributions, but for grains between 1×10^{-17} and 3×10^{-16} kg, a depression is evident. We repeated the analysis for the interstellar grains detected by the Galileo detector. Unlike the Ulysses data, we saw no depression in the mass distribution of the Galileo data (Fig. 1G) obtained between 2 and 4 AU. However, because a large number of grains with masses from 3×10^{-17} to 1×10^{-16} kg have been detected outside 4 AU (77 impacts, see Fig. 1F), these are relatively depleted in the 2- to 4-AU region. The renormalized difference of the histograms (Fig. 1H) reveals that grains are indeed missing from this mass interval. Because the deficiency is in the same mass interval in both the Ulysses and the Galileo data, it is not the result of any special geometry of either of the spacecrafts' orbit. Although the gap in the Ulysses data seems to be broader than that in the Galileo data, the difference in width is not statistically significant. This gap is not a feature of the original interstellar grain mass distribution in the LIC, because it is not present in the data obtained outside 4 AU. Therefore, the gap is a local phenomenon.

Mechanisms that can cause the gap fall into two categories: the destruction of grains exposed to the solar environment, and the diversion of grains by a repelling force originating from the sun. Because the LIC is a warm ($T \approx 6900$ K) interstellar diffuse cloud, possible volatile constituents of LIC dust are returned to the gas phase by thermal sputtering, nonthermal sputtering in interstellar shock fronts, and sporadic heating by far-ultraviolet and extreme ultraviolet (FUV and EUV) photons (*24*). Therefore, evaporation upon exposure to sunlight or to solar wind ion

[1]NASA Johnson Space Center, Mailcode SN2, Houston, TX 77058, USA. [2]European Space Agency (ESA), European Space Operation Center, Robert-Bosch-Strasse 5, 64293 Darmstadt, Germany. [3]Department of Computer and System Sciences, Royal Institute of Technology and Stockholm University, Electrum 230, 164 40 Kista, Sweden. [4]Max-Planck-Institut für Kernphysik, 69117 Heidelberg, Germany. [5]Department of Astronomy, University of Florida, Gainesville, FL 32661, USA.

*To whom correspondence should be addressed (at ESA). E-mail: mlandgra@esoc.esa.de

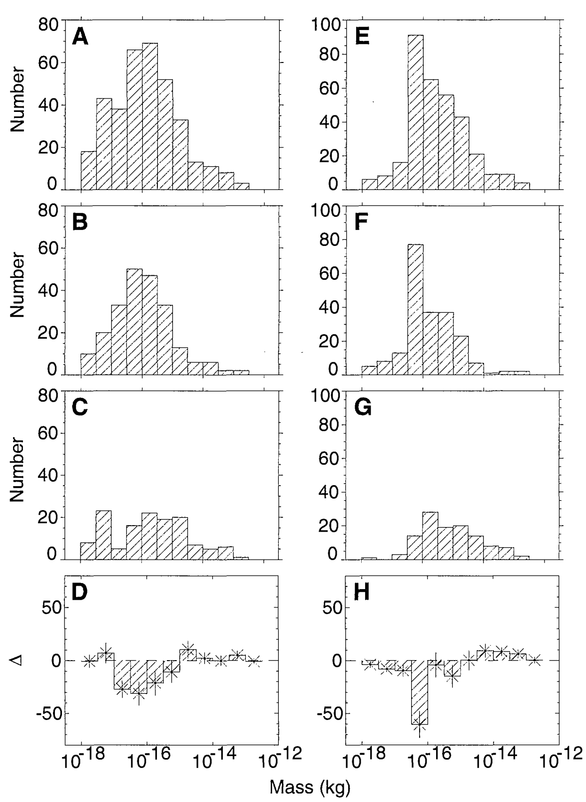

Fig. 1. Mass distributions of interstellar grains measured in situ by Ulysses (**A** to **D**) and Galileo (**E** to **H**). Pairs of panels show the distribution of all detected interstellar grains [as reported by Frisch *et al.* (*8*)] (A and E), the distribution of grains detected outside 4 AU (B and F), the distribution of grains obtained between 2 and 4 AU (C and G), and the differences between the latter two distributions (D and H). Both measurements show that interstellar grains in the mass range from 1×10^{-17} to 3×10^{-16} kg are deficient at heliocentric distances between 2 and 4 AU. The asterisks with vertical lines indicate the statistical 1σ uncertainty of the difference Δ.

impacts does not explain the gap in the grain mass distribution. Although it is possible to conceive of a reasonable interplanetary dust distribution that preferentially causes destruction in the size range of the gap as the two dust populations collide, the interplanetary particle number density is several orders of magnitude too low and causes only a negligible destruction rate (*25*). We are therefore left with diversion by a repelling force as the likely cause of the observed gap.

Given charge levels near +5 V expected on grains in the solar system (*26*), interaction between interstellar grains and the solar wind is dominated by coupling between grain charges and the magnetic field carried by the solar wind, rather than by solar wind ion impacts. The initially radial field lines wrap into an Archimedean spiral as the source region on the sun rotates underneath the radially expanding solar wind. Tightly wrapped magnetic field lines thus become primarily tangential in the outer solar system. The result of the tangential field component carried by the radially expanding wind is an induced electric field that dominates other force components acting on the grain charges (*21*). The 22-year periodicity of the magnetic field causes a perturbation of the grain flow of a magnitude that depends linearly on the charge-to-mass ratio. Grains are pushed toward the solar equatorial plane at times when the solar magnetic field points south, as it did before the 1991 solar maximum. The electric field reverses and pushes the grains away from this plane in the following 11 years. The charge-to-mass ratio–dependent solar wind interactions can lead to complex local distortions of the grain mass distribution that are further complicated by grain inertia.

Solar wind interactions, which can cause either a number enhancement or a deficit, mostly affect smaller grains (mass $< 3 \times 10^{-17}$ kg). If the grains within the mass range of the gap were removed by this mechanism alone, then the smaller grains should be less abundant than grains in the mass range of the gap. This is not compatible with our observations (Fig. 1C), which show an abundance of grains with masses from 1×10^{-18} to 1×10^{-17} kg.

The most promising mass-selection mechanism by which our observations can be explained is the perturbation of dust trajectories by radiation pressure. This preferentially acts on grains according to their size. The ratio of radiation pressure force to gravity, β, reaches a maximum near the mass range of the gap grains (Fig. 2). Mie calculations of β as a function of grain mass for compact spherical grains that consist of astronomical silicates depend on their refractive indices (*27*) and their density. Because β is inversely proportional to the grain density (*28*), it affects the magnitude of β but not the shapes of the curves shown in Fig. 2. Interstellar polarization of starlight shows that the grains causing extinction of starlight are elongated, probably by the ratio 2:1 to 3:1 (*29*). T-matrix calculations of β for elongated grains represented by two spheres in contact are in agreement with the microwave measurements of aggregates at equivalent masses from 10^{-17} to 10^{-16} kg (*30, 31*). These calculations show that the elongation has only a small effect. Particles in the mass range near the gap are expected to be repelled by the sun ($\beta > 1$), whereas grains in all other mass ranges are attracted to the sun ($\beta < 1$) (Fig. 2). Radiation pressure can therefore explain the selective action on grains in the mass range from 1×10^{-17} to 3×10^{-16} kg.

From our interpretation that the deficiency is caused by radiation pressure effects, we conclude that $\beta > 1$ for grains in the mass range that exhibits the deficiency. The first step in estimating the value of β is to assume that grains with $\beta > 1$ can penetrate the solar system to a specific distance from the sun, r_{min}. This minimal distance can be expressed as

$$r_{\min} = \frac{4G(\beta - 1)M_{\odot}}{v_{\infty}^2(1 - \cos\phi)} \qquad (1)$$

(*32*), where ϕ is the angle between the downstream direction vector and the vector to the limiting surface (Fig. 3), v_∞ is the initial grain velocity, G is the gravitational constant, and $M_\odot$ is the solar mass. This function r_{min} defines a rotationally symmetric paraboloid with the sun at the focus (Fig. 3), with the axis of symmetry parallel to the upstream direction of interstellar dust as determined by Baguhl *et al.* (*19*). According to our interpretation, this region around the sun should exhibit the measured deficiency of grains with masses from 1×10^{-17} to 3×10^{-16} kg. Because the deficiency is present in the data obtained between 2 and 4 AU, we conclude that 2 AU $\leq r_{min} \leq$ 4 AU. By inverting Eq. 1, we can estimate β to be $1.4 \leq \beta \leq 1.8$ for grains in the mass range from 1×10^{-17} to 3×10^{-16} kg.

The dependency of β on grain mass can be evaluated for homogeneous spheres and bispheres, but the dependency on shape or internal inhomogeneities (including voids) is much more difficult to evaluate. A consistent picture is emerging from a combination of calculations for cases where a solution can be found and microwave analog laboratory data for complex structures like aggregates (*31*). The geometric cross section/mass ratio dominates the change in β at masses exceeding $\sim 10^{-14}$ kg as long as all particle dimensions exceed a few micrometers. If the wavelength of the incident radiation is comparable to the dimension of the grain or constituents of an aggregate, resonances in the internal electromagnetic field can be triggered. This redistributes the scattered light and therefore affects the momentum deposited in the particle. The result is a radiation force that can exhibit one or several sharp peaks or oscillations near the masses of the gap grains. Voids and other inhomogeneities can lead to either an increase or a decrease in β. The mass range below the gap is better understood, and the asymptotic dependence at low masses is a constant value that is monotonically approached from higher values (*33*). This value is also relatively insensitive to the shape of randomly oriented particles, so that the lower cutoff of the mass gap could indicate the

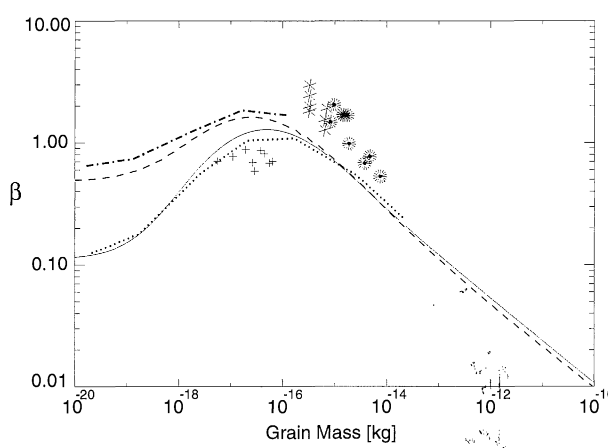

Fig. 2. Ratio of radiation pressure force to gravity, β, as a function of grain mass. The solid curve is for homogeneous spherical "astronomical silicate" grains with an assumed density of 2500 kg m^{-3}. The dotted curve is for two spheres in contact made of the same material after averaging over random orientations. The dashed curve is for spherical grains made of an organic refractory material with an assumed density of 1800 kg m^{-3} (see text). The dash-dot curve is a random-orientation average for sets of two spheres made of the same organic material. Individual points illustrate the effect of more complex particle structures. Pluses denote compact aggregates of tens of spheres made of the "astronomical silicate." Star symbols denote microwave analog data on aggregates of several hundred silicate particles in low-density packing (near 10%) aggregates. The heavy symbols denote the same low-density aggregates after a coating representing organic refractories had been applied (*33*). The data used to produce the curves for homogeneous spheres and bispheres were obtained by integrating across the solar spectrum. The data for porous structures were obtained using data for a single wavelength (λ = 450 nm) at the peak of the solar spectrum and are added for the purpose of illustration only.

particle material. This is illustrated using an organic refractory material (*34*) with an approximate density of 1800 kg m^{-3} (Fig. 2). The refractory material was produced from cosmic abundances condensed on a cold substrate. It was then allowed to evolve in an ambient UV-light field, leading to modification of its chemistry. It is possible that a material of this type mixed with silicates is part of a complex mixture producing the astronomical silicates. A β-induced mass gap would extend to smaller sizes if this material dominates (Fig. 2).

These calculations of the optical properties of interstellar grains can be tested against the range of β values that are consistent with the observed gap in the mass distribution. The average mass density of the grains is a free parameter in this comparison. Less dense grains exhibit a larger optical cross section/mass ratio than more dense grains of the same size. Astronomical silicate grains have the desired β value of 1.6 if the grain density is 2000 kg m^{-3} (spherical) or 1700 kg m^{-3} (elongated). These grain densities are comparable with the densities of constituents of cosmic interplanetary dust particles that were collected in Earth's upper atmosphere [2000 to 2500 kg m^{-3} (*35*)]. Recently it was found (*36*) that the infrared spectrum of one silicate phase of these constituents, called GEMS (glass with embedded metal and sulfides), matches the infrared spectra of dusty interstellar molecular clouds. GEMS are believed to be ancient interstellar grains that were part of the solar nebula in which they were embedded in interplanetary dust particles. The maximum β values for compact organic refractory grains (*34*) are 1.7 (spherical) and 1.9 (elongated). Thus, organic refractory grains are also good candidates for interstellar grains in the mass range of the gap.

Burns *et al.* (*28*) calculated β for compact spherical grains made of various silicates, water ice, iron, magnetite, and graphite. They found $\beta < 1$ for all grain sizes for water ice, amorphous quartz, obsidian, and basalt. Grains that consist of these materials can have β values of 1.6 only if their density is much lower than that of the bulk material. However, at low densities the absorption and scattering efficiency of the material decreases, and hence β cannot be arbitrarily increased by decreasing the grain density. We conclude that grains consisting of the above-mentioned materials cannot account for the observed β-induced deficiency. The maximum β values calculated for compact as well as fractal (*37*) graphite grains are greater than 2. Such high β values create a gap in the grain mass distribution inside 5.2 AU, but no such gap is evident in the data obtained outside 4 AU. Outside the mass range of the gap, however, graphite grains may have lower β values.

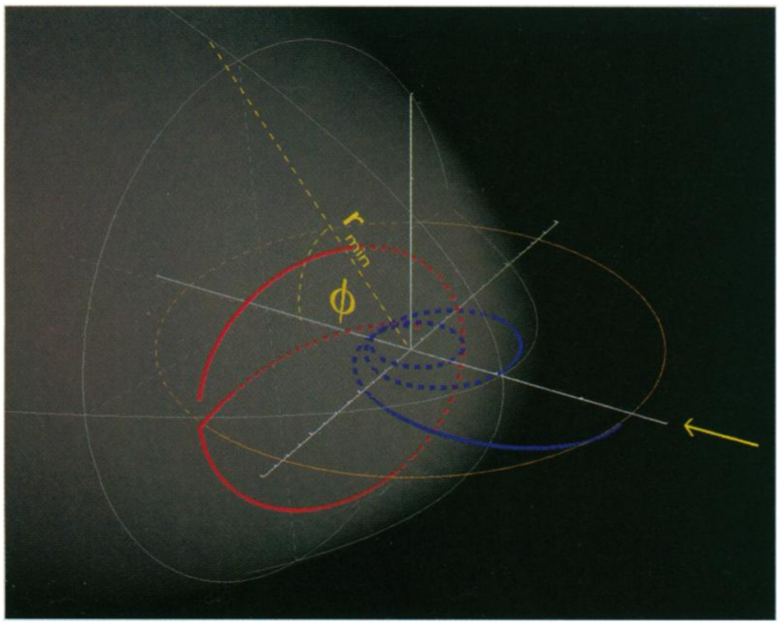

Fig. 3. Three-dimensional geometry of the "forbidden zone" (gray, semitransparent paraboloid object with embedded wire frame), the volume that cannot be entered by interstellar grains with high β values, with respect to the orbits of Ulysses (red) and Galileo (blue) in an ecliptic coordinate system (white; the tick marks show 0.5 AU intervals, the spring point is to the upper right, and the sun is at the center). The orbit of Jupiter is shown as an orange line. The high inclination of 79° of Ulysses' orbit was achieved by a flyby of Jupiter in February 1992 (sharp bend of Ulysses' orbit at Jupiter). The parts of the trajectories that lie inside the forbidden zone are shown as dashed lines. In the measurements along the dashed parts of the trajectories, grains with high β values should be missing. The geometry of the forbidden zone can be described analytically (see Eq. 1) by the distance r_{min} as a function of the angle ϕ, both indicated in yellow. The yellow arrow on the right indicates the stream direction of dust from the LIC as determined by Baguhl *et al.* (*19*). This direction is accidentally close to the ecliptic plane.

References and Notes

1. E. Grün *et al.*, *Astron. Astrophys. Suppl.* **92**, 411 (1992).
2. E. Grün *et al.*, *Space Sci. Rev.* **60**, 317 (1992).
3. E. Grün *et al.*, *Planet. Space Sci.* **43**, 941 (1995).
4. E. Grün *et al.*, *Icarus* **129**, 270 (1997).
5. H. A. Zook *et al.*, *Science* **274**, 1501 (1996).
6. E. Grün *et al.*, *Nature* **362**, 428 (1993).
7. E. Grün *et al.*, *Astron. Astrophys.* **286**, 915 (1994).
8. P. C. Frisch *et al.*, *Astrophys. J.* **525**, 492 (1999).
9. C. S. Weller and R. R. Meier, *Astrophys. J.* **193**, 471 (1974).
10. J. L. Bertaux *et al.*, *Astron. Astrophys.* **150**, 1 (1985).
11. R. Lallement and P. Bertin, *Astron. Astrophys.* **266**, 479 (1992).
12. M. Witte, H. Rosenbauer, H. Banaszkiewicz, H. Fahr, *Adv. Space Res.* **13**, (6)121 (1993).
13. M. Baguhl, E. Grün, M. Landgraf, *Space Sci. Rev.* **78**, 165 (1996).
14. J. L. Bertaux and J. E. Blamont, *Nature* **262**, 263 (1976).
15. J. A. M. McDonnell and O. E. Berg, in *Space Research XV* (Akademie-Verlag, Berlin, 1975), pp. 555–563.
16. E. H. Levy and J. R. Jokipii, *Nature* **264**, 423 (1976).
17. K. W. Behannon *et al.*, *J. Geophys. Res.* **94**, 1245 (1989).
18. B. Å. S. Gustafson and N. Y. Misconi, *Nature* **282**, 276 (1979).
19. M. Baguhl *et al.*, *Science* **268**, 1016 (1995).
20. G. E. Morfill and E. Grün, *Planet. Space Sci.* **27**, 1283 (1979).
21. B. Å. S. Gustafson and S. M. Lederer, in *Physics, Chemistry and Dynamics of Interplanetary Dust*, B. Å. S. Gustafson and M. S. Hanner, Eds. (Astronomical Society of the Pacific, San Francisco, 1996), pp. 35–39.
22. M. Landgraf and E. Grün, in *Proceedings of the IAU Colloquium No. 166*, Garching, Germany, 21 to 25 April 1997, D. Breitschwerdt, M. J. Freyberg, J. Trümper, Eds., vol. 506 of *Lecture Notes in Physics* (Springer, Heidelberg, 1998), pp. 381–384.
23. The data sets contain data from 804 days of Ulysses measurements between 2 and 4 AU and 822 days outside 4 AU. Galileo spent 598 days between 2 and 4 AU and 632 days outside 4 AU before it arrived at Jupiter. To compare the 2- to 4-AU and >4-AU mass histograms, we scale the 2- to 4-AU histogram of the Ulysses data by 822/804 and the 2- to 4-AU histogram of the Galileo data by 632/598.
24. A. P. Jones *et al.*, *Astrophys. J.* **433**, 797 (1994).
25. If the spatial density of interplanetary particles in the 2- to 4-AU region is 10^{-5} m^{-3}, 3 of 10^6 interstellar grains are destroyed by a collision in this region.
26. T. Mukai, *Astron. Astrophys.* **99**, 1 (1981).
27. B. T. Draine and H. M. Lee, *Astrophys. J.* **285**, 89 (1984).
28. J. A. Burns, P. L. Lamy, S. Soter, *Icarus* **40**, 1 (1979).
29. A. Li and J. M. Greenberg, *Astron. Astrophys.* **323**, 566 (1997).
30. M. I. Mischenko, *Appl. Opt.* **32**, 4652 (1993).
31. Y. Xu and B. Å. S. Gustafson, *Astrophys. J.* **513**, 894 (1999).
32. M. Landgraf, M. Müller, E. Grün, *Planet. Space Sci.* **47**, 1029 (1999).
33. B. Å. S. Gustafson, *Annu. Rev. Earth Planet. Sci.* **22**, 553 (1994).
34. J. M. Greenberg *et al.*, *Astrophys. J.* **455**, L177 (1995).
35. D. E. Brownlee *et al.*, in *Proceedings of the 6th Lunar Science Conference*, Houston, TX, 17 to 21 March 1975 (Pergamon, New York, 1975), pp. 3409–3416.
36. J. P. Bradley *et al.*, *Science* **285**, 1716 (1999).
37. T. Mukai, T. Kozasa, J. Blum, J. M. Greenberg, *Astron. Astrophys.* **262**, 315 (1992).

38. We thank A. L. Graps for improving the clarity of the text. This work was performed while M.L. held a position funded by the program on physics of star formation at the Deutsche Forschungsgemeinschaft. We also thank M. Mischenko for making his T-matrix light scattering code for bispheres available, Y.-L. Xu for calculating scattering by bispheres and larger clusters of spheres using his boundary condition code, and L. Kolokolova for performing the T-matrix light scattering calculations for bispheres. Supported in part by NASA grant NAG5-6378.

21 July 1999; accepted 28 October 1999

LINKED CITATIONS

You have printed the following article:

Deflection of the Local Interstellar Dust Flow by Solar Radiation Pressure
M. Landgraf; K. Augustsson; E. Grun; B. A. S. Gustafson
Science, New Series, Vol. 286, No. 5448. (Dec. 17, 1999), pp. 2319-2322.
Stable URL:
http://links.jstor.org/sici?sici=0036-8075%2819991217%293%3A286%3A5448%3C2319%3ADOTLID%3E2.0.CO%3B2-X

This article references the following linked citations:

References and Notes

[5] **Solar Wind Magnetic Field Bending of Jovian Dust Trajectories**
H. A. Zook; E. Grun; M. Baguhl; D. P. Hamilton; G. Linkert; J.-C. Liou; R. Forsyth; J. L. Phillips
Science, New Series, Vol. 274, No. 5292. (Nov. 29, 1996), pp. 1501-1503.
Stable URL:
http://links.jstor.org/sici?sici=0036-8075%2819961129%293%3A274%3A5292%3C1501%3ASWMFBO%3E2.0.CO%3B2-S

[19] **Dust Measurements at High Ecliptic Latitudes**
M. Baguhl; D. P. Hamilton; E. Grun; S. F. Dermott; H. Fechtig; M. S. Hanner; J. Kissel; B.-A. Lindblad; D. Linkert; G. Linkert; I. Mann; J. A. M. McDonnell; G. E. Morfill; C. Polanskey; R. Riemann; G. Schwehm; P. Staubach; H. A. Zook
Science, New Series, Vol. 268, No. 5213. (May 19, 1995), pp. 1016-1019.
Stable URL:
http://links.jstor.org/sici?sici=0036-8075%2819950519%293%3A268%3A5213%3C1016%3ADMAHEL%3E2.0.CO%3B2-F

[36] **An Infrared Spectral Match between GEMS and Interstellar Grains**
John P. Bradley; Lindsay P. Keller; Theodore P. Snow; Martha S. Hanner; George J. Flynn; Joseph C. Gezo; Simon J. Clemett; Donald E. Brownlee; Janet E. Bowey
Science, New Series, Vol. 285, No. 5434. (Sep. 10, 1999), pp. 1716-1718.
Stable URL:
http://links.jstor.org/sici?sici=0036-8075%2819990910%293%3A285%3A5434%3C1716%3AAISMBG%3E2.0.CO%3B2-W

NOTE: *The reference numbering from the original has been maintained in this citation list.*